

Photoelectrochemical Properties of Nanostructured Copper Oxides Formed Sonoelectrochemically

P. Grez^{1,*}, C. Rojas¹, I. Segura¹, C. Heyser¹, L. Ballesteros², C. Celedón³, and R. Schrebler¹

¹ Instituto de Química, Pontificia Universidad Católica de Valparaíso, Avda. Universidad 330, Curauma, Placilla, Valparaíso Casilla, 4059 Valparaíso, Chile

² Laboratorio de Síntesis Inorgánica y Electroquímica, Facultad de Ciencias, Universidad de Chile. Las Palmeras#3425, Ñuñoa, Santiago-Chile

³ Departamento de Física, Universidad Técnica Federico Santa María, P.O. Box 110-V, Valparaíso, Chile

*E-mail: paula.grez@pucv.cl

Received: 24 March 2017 / Accepted: 28 May 2017 / Published: 12 July 2017

In this work nanostructured copper oxides (Cu_xO) were prepared by ultrasound-assisted anodization of copper foils. These Cu_xO nanostructures were characterized morphologically and structurally by SEM and XRD, respectively. The bandgap value was determined by diffuse reflectance measurements. The electrochemical characterization included Mott Schottky plots and electrochemical techniques. From these measurements it was possible to establish that the formed phase corresponded to p- Cu_2O . The best results in the cathodic photocurrent response for the system $\text{Cu}|\text{p-Cu}_2\text{O}|10 \text{ mM KI}, 1 \text{ mM KI}_3$ in $50 \text{ mM Na}_2\text{B}_4\text{O}_7$ (pH 9.2) were obtained with oxides prepared at 75°C , 100V in ethylene glycol contained 5% wt H_2O and 0.5 wt% NH_4Cl .

Keywords: nanostructured copper oxides, sonoelectrochemical synthesis, photoelectrochemical properties

1. INTRODUCTION

Quasi-unidimensional (Q1D) nanostructured materials have a higher surface area/volume ratio [1-3] offering better crystallinity, higher integration density, lower power consumption and a decrease of the recombination process, due to the less distance that the photogenerated charge carriers must travel to attain the interface [4]. In addition, due to its size confinement renders tunable band gap, higher optical gain and faster operation speed [5]. Thus, these nanomaterials are being applied in

different areas, such as, in cosmetics, pharmaceuticals, electronics [2] and in photovoltaic and photoelectrochemical devices [6].

One of these cases is the manufacture of nanostructures for energy storage and production of fuels with a high relation between produced energy/CO₂ emissions. An example of the latter is hydrogen production [7]. Synthesis methods are fundamental for nanostructures formation. The methods more often used are physical (laser ablation, arc-discharge and evaporation) and chemical (thermal decomposition of precursor compound, chemical deposition and electroformation). Chemical methods had shown be more effective, they provide a better control of nanostructure formation getting adequate shapes and sizes. In the recent years, there are too many improvements for both conditions control and experimental techniques [8]. Ultrasound irradiation coupled with chemical methods had shown to be a convenient way for manipulate the size and shape of nanostructured materials (Q1D structures like nanowires, nanoneedles, nanorods, nanobelts and nanotubes). These techniques are called Sonochemical [9-17] and Sonoelectrochemical [2, 18-26].

The chemical effects of the use of ultrasound coupled with chemical methods arise primarily from the acoustic cavitation phenomena which involve the formation, growing and implosive collapse of bubbles into a liquid media [2, 9, 11, 13, 25]. The implosive collapse of the bubble near the solid surface generates a strong current towards the solid surface, increasing the mass flow on the nanotubular surface. The quality of the nanotubes generated through the use of ultrasound would present a better quality because the mass transfer is uniform during the formation process [19]. This phenomenon had been used for the preparation of various inorganic nanomaterials as metals, chalcogenides, nanocomposites and metallic oxides among others [9, 13, 25, 27].

In recent years, studies related the sonoformation of metallic oxide semiconductor nanotubes, mainly TiO₂ [17, 21] and Fe₂O₃ [21, 22, 28, 29] for their applications as photoelectrode in photoelectrochemicals cells (PEC). However, although copper oxides semiconductors (Cu_xO, x = 1 or 2) have been topics of study at the last decade for their diverse properties: (a) Narrow band gap values, E_g = 1.20 eV [30] for CuO and 2.1 eV [31] for Cu₂O; (b) could be synthesized by both, chemical and electrochemical methods, considering the latter as economically superior and cleaner methods; (c) exhibit good semiconductor behavior, low toxicity and relative abundance at the Earth crust [32] and (d) they have an adequate stability in common aqueous electrolyte, the formation of Cu_xO nanostructures has not been extensively studied through techniques such as sonoelectrochemical.

In this way, the main object of this investigation is the study of the sonoelectrochemical synthesis and characterization of the electrical properties of p-Cu_xO nanostructures, which could be used in the near future as photocathodes in photoelectrochemical and in photovoltaic solar cells.

2. EXPERIMENTAL SECTION

2.1 Synthesis

Nanostructured copper oxides layers have been electrochemically grown by ultrasound-assisted anodization of copper foils (Sigma-Aldrich, 99.98%, 0.25 mm) at three potential values of 50 V, 75 V and 100 V in ethylene glycol (EG; 99.8%, anhydrous), ammonium chloride (0.5 wt% NH₄Cl) and 3.0% wt ≤ [H₂O] ≤ 15% wt. The anodization experiments were carried out using ultrasonic waves (36

kHz, 60 W) for a time period of 900 s. The temperatures of the bath were 50°C and 75°C. The above process was carried out using a two electrode system (flag shaped 1.0 cm² Cu foil as anode and carbon plate, 22.55 cm² as cathode; the distance between cathode and anode was kept at 3 cm).

2.2 Characterization

Cu_xO nanostructures were characterized by scanning electron microscopy (SEM). The images were obtained on a Zeiss model EVO MA 10 with an EDS Penta FET Precision detector, Oxford Instruments X-ac. X-ray diffraction (XRD) was used to structurally characterize the nanostructured Cu_xO, employing an X-ray diffractometer, Bruker model D8 Advance, using Cu K α radiation. The accelerating voltage was settled at 40 KV with a 25mA flux. Reflectance Diffuse measurement was carrying out using UV-2600, UV-Vis Spectrophotometers between 826.5 to 300 nm. The optical bandgap (E_g) value of the samples was measured at room temperature and front of air.

The Mott Schottky plots were realized with a Zahner, model IM6e, potentiostat/galvanostat equipped with Thales software. A conventional three-electrode electrochemical cell was used. A platinum wire and an Ag/AgCl_{sat} (0.197 V vs HNE) were employed as auxiliary and reference electrodes, respectively. For lineal voltammetry scan and photocurrent transients measurements the same conventional three-electrode electrochemical cell and Ecochimie potentiostat/galvanostat, Autolab PGSTAT100 model were used. Electrolyte solution contained 10 mM KI, 1 mM KI₃ in 50 mM Na₂B₄O₇ (pH 9.2) solution. Under illumination conditions a 1000 W Hg:Xe 6295 ORIEL INSTRUMENTS lamp was employed.

3. RESULTS AND DISCUSSION

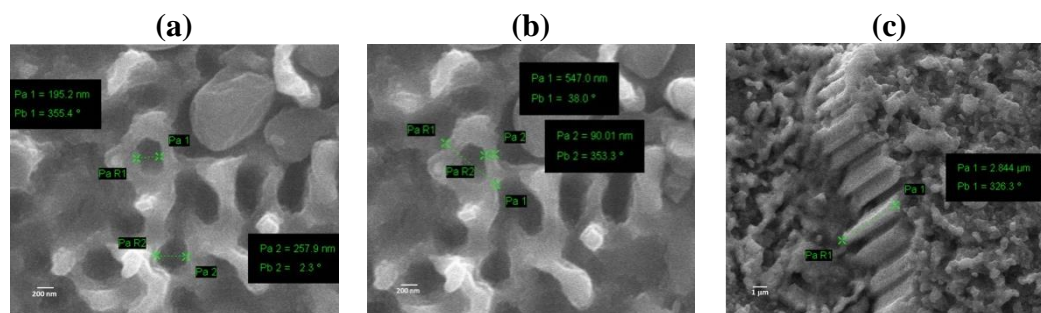


Figure 1. (a) and (b) top view SEM images and (c) the cross-sectional tilt SEM image, tilt angle of 45° of Cu_xO nanostructures grown by ultrasound-assisted anodization of copper substrates, at 75°C, 100V in ethylene glycol contained 5% wt H₂O and 0.5wt% NH₄Cl.

First, is important to clarify that for experimental conditions of 3% wt and 15% wt H₂O, no nanostructures were obtained in the polarization time tested (900 s). For this reason the discussion will focus on the other two conditions (5% wt and 10% wt H₂O).

Figures 1a-b show SEM images of Cu_xO nanostructures samples, electrochemically grown by ultrasound-assisted anodization of copper substrates at 75°C, 100V in ethylene glycol contained 5% wt H₂O and 0.5% wt NH₄Cl. The nanoporous sample (see Fig. 1a-b) is characterized by pores of a mean

diameter of 547 nm, an inner diameter of approximately 227 nm and a length of 2.8 μm (Fig. 1c). Similar images were obtained at 75°C at 50V and 100V in solutions with 5% wt and 10% wt of H_2O . For those experiments performed at 50°C in all conditions, SEM images showed a growth of nanorod where the height and diameter were small, i.e. with a low aspect ratio.

From the observation of the cross-sectional tilt SEM image (see Fig. 1c) one could say that there is a laminar growth with some clear openings on the ends typical for nanotubes.

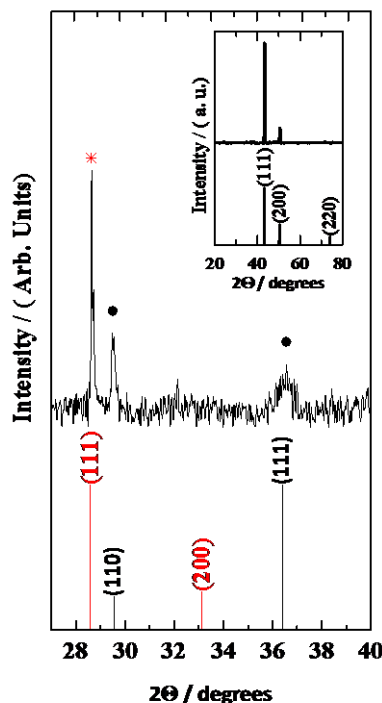


Figure 2. X-ray diffraction pattern of a Cu_2O nanostructured sample grown at same conditions indicated in Fig. 1. Cubic Cu_2O JCPDS pattern (#05-0667) and Cubic CuCl JCPDS pattern (#06-0334) are also shown for comparison (black and red lines, respectively). • Cu_2O and * CuCl . The inset shows X-ray diffraction pattern of copper substrate (Cu pattern JCPDS 04-0836).

In order to study the structural properties of the Cu_xO nanostructures grown on copper foil, X-ray diffraction experiments have been carried out. Figure 2 shows the XRD pattern for Cu_xO nanostructured grown in the conditions indicated in Figure 1. Two diffraction peaks appearing at $2\Theta = 29.54^\circ$ and 36.58° that correspond to (110) and (111) planes of cubic Cu_2O , respectively, according to JCPDS card No. 05-0667. It also shows a peak corresponding to a secondary phase of CuCl , according to JCPDS card No. 06-0334. In the XRD pattern there are not evidences of impurities attributed to Cu (II) compounds such as CuO or CuCl_2 . Moreover, the presence of two peaks in the diffraction pattern is indicative of the polycrystalline nature of the Cu_2O nanostructures. However, this nanostructure shows a preferential growth along the [110] and [111] directions.

On the other hand, when the XRD pattern was recorded at values of $2\Theta > 40^\circ$, it is showed only the signals corresponding to copper substrate such as seen in the inset of Fig. 2. Similar XRD patterns were recorded for the samples obtained in all experimental conditions tested.

In order to determine some of the semiconductor characteristic parameters of the Cu_2O nanostructures, the variation of the interfacial capacitance with potential was extracted from

electrochemical impedance measurements at high frequency (10 kHz) in a 50 mM $\text{Na}_2\text{B}_4\text{O}_7$ (pH 9.20) solution at inert atmosphere. The capacitance variation of the Cu_2O nanostructures with potential was recorded in the potential range from 0.00 V to 1.00 V in darkness and without stirring. For these measurements a Faraday cage and Pt tip connected to the reference electrode using a 10 mF capacitor were used in order to reduce the noise and error of the measurements at high frequencies, respectively.

Figure 3a shows a negative slope indicating the p-type electrical conductivity of Cu_2O nanostructures [33]. An apparent carrier majority density (N_A) of $1.98 \times 10^{19} \text{ cm}^{-3}$ was determined from the slope of the plot of Fig. 3a (assuming 6.3 as the dielectric constant of Cu_2O [34]) has been obtained, and the extrapolation of the straight line to $1/C^2 = 0$ gives for Cu_2O a flat band potential, $E_{\text{FB}} = 0.238 \text{ V}$. The E_{FB} values and apparent density of majority charge carriers are similar to those determined by other authors. However, the observed differences in carrier density can be attributed to different real areas of nanostructures exposed to the interface [35].

Figure 3b shows the optical bandgap energy (E_g), for the Cu_2O nanostructures grown in the same experimental conditions as those detailed in figure 1, which was determined by reflectance diffuse measurement. The obtained E_g value was ca. 2.26 eV and corresponded to a direct transition, similar results have been reported by other authors [31]. In all other experimental conditions the band gap value was similar, obtaining an average value of $E_g = 2.21 \pm 0.08 \text{ (eV)}$. Furthermore, from the semiconductor parameters (E_{FB} and N_A) and optical one (E_g) obtained above, the energy band diagram has been constructed and is depicted in Fig. 3c for a p- Cu_2O nanostructured sample obtained in the conditions indicated in Fig. 1.

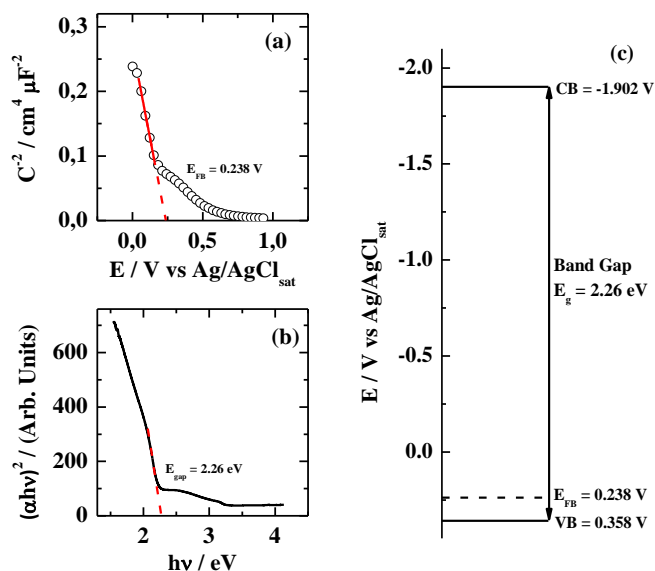


Figure 3. (a) Mott–Schottky plots measured at 10 kHz for a Cu_2O nanostructured electrode in quiescent solution at pH 9.2 (50 mM $\text{Na}_2\text{B}_4\text{O}_7$), in the absence of light and inert atmosphere. (b) Band gap value from diffuse reflectance measurements (c) Energy band diagram of the system.

Figure 4a shows potentiodynamic j/E profiles of the Cu_2O nanostructures electrodes obtained under dark and illumination with continued and chopped white light.

It is observed type-p behaviour when the electrode is illuminated in accord with Mott Shottky results (see Fig. 3a). Furthermore, for these electrodes, the photocurrent potential onset (E_{bph}), is achieved at a potential value of -0.20 V. However, when considering the respective E_{FB} values, it can be observed that the overpotential η , ($\eta = E_{bph} - E_{FB}$) attained to ~ -0.438 V value. This relatively high η value could be explained due to the energy requirements for the charge transfer process of the coupling (I_3^-/I^-) on this electrode type. On the other hand, the photocurrent under chopped light illumination presents a value equal to that obtained with continued light illumination and a low level of recombination. This last, is reflected by the low photocurrent decay after each light pulse.

Photocurrent transients (PT) measurements were carried out in order to verify the level of recombination of photogenerated charge carriers, these were realized following the methodology of L. Peter [36]. Figure 4b shows the square wave chopped light perturbation program applied to the Cu_2O photoelectrode employed during this type of PT studies. Figure 4c-d shows the behaviour of experimental photocurrent transient at polarization potential of -0.32 V and -0.36 V, respectively. In the interval between $t = 0$ and $t = 1$ a decay of the photocurrent can be observed until to reach a steady state value ($j_{ph,st}$). This stationary current is a balance between the charge transfer and recombination processes.

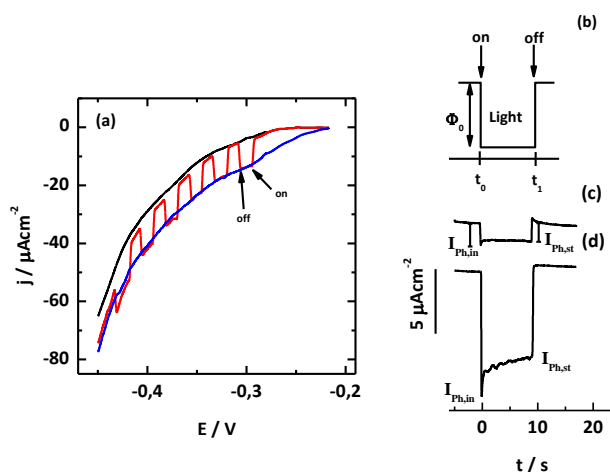


Figure 4. (a) Linear scan voltammetry of Cu_2O nanostructures electrodes in the dark (black line), with continuous light illumination (blue line) and under chopped light illumination conditions (red curve). These curves have been recorded at $v = 0.010$ Vs^{-1} (b) Light pulse waveform used for photocurrent transient measurements. Photocurrent transients obtained at (c) $-0.32V$ and (d) $-0.36V$. These results were obtained with Cu_2O nanostructures electrodes (sample grown at same conditions indicated in Fig. 1) in 10 mM KI , 1 mM KI_3 in 50 mM $Na_2B_4O_7$ (pH 9.2) solution and room temperature. Light intensity $\Phi_0 = 50.0$ $mWcm^{-2}$.

In this way and considering the relation $j_{ph,st}/j_{ph,in}$ a value close to one will correspond to a system where the charge transference process is favoured with respect to the process of recombination of the charge carriers [37, 38]. This behaviour is observed in our case, where values of this relation were 0.8 and 0.7 for the samples polarized at -0.32 V and -0.36 V, respectively. The results obtained in other experimental conditions are summarized in Table 1.

Table 1. Results obtained for the $j_{ph, st}/j_{ph, in}$ ratio from the photocurrent transients measurements for the p - Cu₂O phase by ultrasound-assisted anodization of copper substrates.

Synthesis Temperature 50°C						Synthesis Temperature 75°C					
Cu ₂ O Synthesis Conditions		E_{pot} / V^*	$j_{ph, in} / \mu Acm^{-2}$	$j_{ph, st} / \mu Acm^{-2}$	$j_{ph, st}/j_{ph, in}$	Cu ₂ O Synthesis Conditions		E_{pot} / V^*	$j_{ph, in} / \mu Acm^{-2}$	$j_{ph, st} / \mu Acm^{-2}$	$j_{ph, st}/j_{ph, in}$
50V	5%	-0.32	-2,17	-0,54	0,25	50V	5%	-0.32	-12,12	-5,49	0,45
		-0.36	-3,44	-2,09	0,61			-0.36	-20,37	-15,91	0,78
	10%	-0.32	-6,40	-0,82	0,13		10%	-0.32	-2,21	-0,92	0,42
		-0.36	-7,04	-1,07	0,15			-0.36	-2,29	-1,52	0,66
75V	5%	-0.32	-2,00	-0,80	0,40	75V	5%	-0.32	-18,10	-5,48	0,30
		-0.36	-2,80	-1,03	0,37			-0.36	-19,24	-9,64	0,50
	10%	-0.32	-3,49	-1,42	0,41		10%	-0.32	-2,10	-1,15	0,55
		-0.36	-4,86	-2,85	0,59			-0.36	-1,98	-0,72	0,36
100V	5%	-0.32	-	-	-	100V	5%	-0.32	-1,97	-1,60	0,81
		-0.36	-8,47	-4,52	0,53			-0.36	-10,14	-6,76	0,67
	10%	-0.32	-2,38	-1,29	0,54		10%	-0.32	-	-	-
		-0.36	-2,16	-0,96	0,44			-0.36	-	-	-

*Potential value vs Ag/AgCl_{sat} (0.197 V vs HNE)

From the analysis of Table 2, it is established that although in general the samples obtained show a relation $j_{ph, st} / j_{ph, in}$ close to 0.5 or higher, the nanostructures that show a better behaviour like photocathodes are those obtained at 100V, 75°C and with 5% wt H₂O, the above is due to the fact that they present a higher initial and stationary photocurrent value. In this way, it can be determined that there are more minority carriers (electrons) to be used in the photoreduction of a reaction of interest. The last means that in the Cu₂O nanostructures samples assayed the rate of Faradic process is higher than the rate of the recombination process [33, 39-41]. This could establish that the most of photogenerated charges were used in the photo-reduction process ($I_3 + 2e^- \rightarrow 3I^-$)

4. CONCLUSIONS

From the above discussion, was obtained Cu₂O nanostructures in the experimental conditions tested. Those grown at 75°C, 100V in ethylene glycol contained 5% wt H₂O and 0.5 wt% NH₄Cl, were those with better photoelectrochemical behaviour. However, from the SEM images and the XRD spectrum it was possible to conclude that the polarization times should be less than 900 s. This last, is due to the growth of a film, possibly of CuCl, that is forms at the upper of the Cu₂O nanostructures, covering part of the electrode surface. This could reduce the photoelectrochemical properties of the Cu₂O nanotubes formed. On the other hand, the energy band diagram shows that the system Cu|p-Cu₂O|50 mM Na₂B₄O₇ (pH 9.2) could be potentially employed as photocathode in the hydrogen evolution reaction in aqueous solutions ($E_{H_2O/H_2} \leq -0.8 V$ vs Ag / AgCl_{sat}).

ACKNOWLEDGEMENTS

The financial support of Fondecyt-Chile (Project N° 1140963) and DI-PUCV (Projects N° 125.789/2014) is gratefully acknowledged by the authors.

References

1. R. Vijaya Kumar, R. Elgamiel, Y. Diamant, A. Gedanken, *Langmuir*, 17 (2001) 1406.
2. V. Sáez, T.J. Mason, *Molecules*, 14 (2009) 4284.
3. J. Bisquert, *Phys. Chem. Chem. Phys.*, 10 (2008) 49.
4. T. Zhang, Z.U. Rahman, N. Wei, Y. Liu, J. Liang, and D. Wang, *Nano Res.*, 10 (2017) 1021.
5. J.G. Lu, P. Chang, Z. Fan, *Mat. Sci. Eng. R*, 52 (2006) 49.
6. S. Lee, C.-W. Liang, and L.W. Martin, *ACS Nano*, 5 (2011) 3736.
7. J. Nowotny, C.C. Sorrell, L.R. Sheppard, T. Bak, *Int. J. Hydrogen. Energ.*, 30 (2005) 521.
8. C.N.R. Rao, S.R.C. Vivekchand, K. Biswas, A. Govindaraj, *Dalton T.*, 34 (2007) 3728.
9. N.A. Dhas, C.P. Raj, A. Gedanken, *Chem. Mater.*, 10 (1998) 1446.
10. N.A. Dhas, C.P. Raj, A. Gedanken, *Chem. Mater.*, 10, 3278 (1998).
11. R.V. Kumar, R. Elgamiel, Y. Diamant, A. Gedanken, *Langmuir*, 17 (2001) 1406.
12. N.A. Dhas, K.S. Suslick, *J. Am. Chem. Soc.*, 127 (2005) 2368.
13. X. Tao, L. Sun, Y. Zhao, *Mater. Chem. Phys.*, 125 (2011) 219.
14. R. Ranjbar-Karimi, A. Bazmandegan-Shamili, A. Aslani, K. Kaviani, *Physica B*, 405 (2010) 3096.
15. S. Anandan, G.J. Lee, J.J. Wu, *Ultrason. Sonochem.*, 19 (2012) 682.
16. V. Safarifard, A. Morsali, *Ultrason. Sonochem.*, 19 (2012) 823.
17. A. Shui, W. Zhu, L. Xu, D. Qin, Y. Wang, *Ceram. Int.*, 39 (2013) 8715.
18. R.G. Cornpton, J.C. Eklund, F. Marken, *Electroanal.*, 9 (1997) 509.
19. S.K. Mohapatra, M. Misra, V.K. Mahajan, K.S. Raja, *J Catal.*, 246 (2007) 362.
20. V. Mancier, A.L. Daltin, D. Leclercq, *Ultrason. Sonochem.*, 15 (2008) 157.
21. S.K. Mohapatra, S.E. John, S. Banerjee, M. Misra, *Chem. Mater.*, 21 (2009) 3048.
22. Z. Zhang, Md.F. Hossain, T. Takahashi, *Mater. Lett.*, 64 (2010) 435.
23. L.-X. Sang, Z.Y. Zhang, C.F. Ma, *Int. J. Hydrogen. Energ.*, 36 (2011) 4732.
24. L.-X. Sang, Z. Zhi-Yu, B. Guang-mei, D. Chun-xu, M. Chong-fang, *Int. J. Hydrogen. Energ.*, 37 (2012) 854.
25. P. Sakkas, O. Schneider, S. Martens, P. Thanou, G. Sourkouni, Chr. Argiris, *J. Appl. Electrochem.*, 42 (2012) 763.
26. J. González-García, V. Sáeza, M.D. Esclapeza, P. Bonetea, Y. Vargas, L. Gaete, *Phys. Procedia*, 3 (2010) 117.
27. S.K. Mohapatra, M. Misra, V.K. Mahajan, K.S. Raja, *Mater. Lett.*, 62 (2008) 1772.
28. T.J. LaTempa, X. Feng, M. Paulose, C.A. Grimes, *J. Phys. Chem. C*, 113 (2009) 16293.
29. R. Schrebler, L.A. Ballesteros, H. Gómez, P. Grez, R. Córdova, E. Muñoz, R.A. Schrebler, J.R. Ramos-Barrado, and E.A. Dalchiele, *J. Electrochem. Soc.*, 161 (2014) H903.
30. J.G. Lu, P. Chang, Z. Fan, *Mat. Sci. Eng. R*, 52 (2006) 49.
31. G. Li, Y. Huang, Q. Fan, M. Zhang, Q. Lan, X. Fan, Z. Zhou, C. Zhang, *Ionics*, 22 (2016) 2213.
32. Q. Pan, M. Wang, *J. Electrochem. Soc.*, 155 (2008) A452.
33. P. Grez, F. Herrera, G. Riveros, R. Henríquez, A. Ramírez, E. Muñoz, E.A. Dalchiele, C. Celedón, R. Schrebler, *Mater. Lett.*, 92 (2013) 413.
34. S. Wu, Z. Yin, Q. He, X. Huang, X. Zhou, and H. Zhang, *J. Phys. Chem. C*, 114 (2010) 11816.
35. Md. A. Hossain, R. Al-Gaashani, H. Hamoudi, M.J. Al Marri, I.A. Hussein, A. Belaidi, B.A. Merzougui, F.H. Alharbi, N. Tabet, *Mat. Sci. Semicon. Proc.*, 63 (2017) 203.
36. L.M. Peter, *J Solid State Electr.*, 17 (2013) 315.
37. P. Salvador, *J. Phys. Chem.*, 89 (1985) 3863.
38. P. Salvador, M.L. García-González, and F. Muñoz, *J. Phys. Chem.*, 96 (1992) 10349.
39. P. Grez, F. Herrera, G. Riveros, A. Ramírez, R. Henríquez, E. Dalchiele, and R. Schrebler, *Phys. Status Solidi A*, 209 (2012) 2470.

40. F.V. Herrera, P. Grez, R. Schrebler, L.A. Ballesteros, E. Muñoz, R. Córdova, H. Altamirano, and E.A. Dalchiele, *J. Electrochem. Soc.*, 157 (2010) D302.
41. R.S. Schrebler, H. Altamirano, P. Grez, F.V. Herrera, E.C. Muñoz, L.A. Ballesteros, R. A. Córdova, H. Gómez, and E.A. Dalchiele, *Thin Solid Films*, 518 (2010) 6844

© 2017 The Authors. Published by ESG (www.electrochemsci.org). This article is an open access article distributed under the terms and conditions of the Creative Commons Attribution license (<http://creativecommons.org/licenses/by/4.0/>).